Title

A free-standing lithium phosphorus oxynitride thin film electrolyte promotes uniformly dense lithium metal deposition with no external pressure

Journal

Nature Nanotechnology, 18(12)

ISSN

1748-3387

Authors

Cheng, Diyi

Wynn, Thomas

Lu, Bingyu

et al.

Publication Date

2023-12-01

DOI

10.1038/s41565-023-01478-0

A free-standing lithium phosphorus oxynitride thin film electrolyte promotes uniformly dense lithium metal deposition with no external pressure

Diyi Cheng[1], Thomas Wynn[1], Bingyu Lu[2], Maxwell Marple[3], Bing Han[2], Ryosuke Shimizu[2], Bhagath Sreenarayanan[2], Jeffery Bickel[4], Peter Hosemann[4], Yangyuchen Yang[1], Han Nguyen[2], Weikang Li[2], Guomin Zhu[2], Minghao Zhang[2,*], Ying Shirley Meng[1,2,5*]

[1]Materials Science and Engineering Program, University of California San Diego, La Jolla, CA 92121, USA
[2]Department of NanoEngineering, University of California San Diego, La Jolla, CA 92121, USA
[3]Physical and Life Science Directorate, Lawrence Livermore National Laboratory, Livermore, CA 94550, USA
[4]Nuclear Engineering Department, University of California Berkeley, Berkeley, CA 94720, USA
[5]Pritzker School of Molecular Engineering, University of Chicago, Chicago, IL 60637, USA

*Corresponding Author E-mails: miz016@eng.ucsd.edu, shirleymeng@uchicago.edu

Abstract

Lithium phosphorus oxynitride (LiPON) is an amorphous solid electrolyte that has been extensively studied over the last three decades. Despite the promise of pairing it with various electrode materials, LiPON's rigidity and air sensitivity set limitations to understanding its intrinsic properties. Here we report a methodology to synthesize LiPON in a free-standing form that manifests remarkable flexibility and a Young's modulus of ~33 GPa. We use solid-state nuclear magnetic resonance and differential scanning calorimetry to quantitatively reveal the chemistry of the Li/LiPON interface and the presence of a well-defined LiPON glass-transition temperature of 207 °C. Combining interfacial stress and a gold seeding layer, our free-standing LiPON shows a uniformly dense deposition of lithium metal without the aid of external pressure. This free-standing LiPON film offers opportunities to study fundamental properties of LiPON for interface engineering for solid-state batteries.

Introduction

One of the long-lasting debates on the fundamental understanding of LiPON material pertains to the N bonding structure and its impact on the lithium transport properties. Early studies on the chemistry of LiPON primarily relied on X-ray photoelectron spectroscopy (XPS), where peak assignments have been disputed based on different hypothesis.[1–3] Alternative methods suitable for probing the local bonding environment, such as neutron paired distribution function (PDF) and solid-state nuclear magnetic resonance (ss-NMR), have previously been unable to validate existing hypothesis due to the difficulty of obtaining a high enough signal-to-noise (S/N) ratio in the presence of the LiPON's substrate. Nevertheless, Lacivita et al. managed to obtain sufficient sample for neutron PDF measurements by scraping LiPON from the substrate.[3] Another aspect of LiPON research lies at its interfaces with various electrode materials. Despite some recent knowledge gained on LiPON-associated interfaces,[4–8] the electrochemomechanical properties of such interfaces appear not to have been explored, although these could serve as critical metrics determining mechanical behaviors at the interface that affects battery cycling.[9] Nevertheless, due to the presence of substrates, the limited methodologies for studying the mechanical properties of LiPON have also created some ambiguity in literature.[10,11]

The dilemma associated with the substrate and the lack of active material for measurements originates from the conventional synthesis methods of LiPON thin film. In fact, a variety of methods are available to synthesize LiPON besides radio frequency (RF) sputtering.[2,12–19] (**Extended Date Table 1**). Methods that get around the use of substrate, such as ammonolysis, plasma synthesis or ball milling, suffer from either altered LiPON properties or the introduction of interfacial impedance between LiPON particles.[17–19]

In this work, we introduce a different methodology to synthesize a LiPON thin film that is in free-standing form without a rigid solid substrate. By leveraging the form factor of this flexible free-standing LiPON (FS-LiPON) thin film, fundamental insights have been obtained from characterizations by ss-NMR, differential scanning calorimetry (DSC) and nanoindentation. With the presence of interfacial stress at Cu/FS-LiPON interface and the introduction of a gold seeding layer, we further demonstrate electrochemical deposition of uniform and fully dense Li metal under zero external pressure, which provides fresh perspectives on interface engineering in bulk Li metal solid-state batteries.

A Flexible Free-standing LiPON Thin Film

Fig. 1a depicts the fabrication procedure of FS-LiPON. Before undertaking RF sputtering, a spin-coating method was used to coat a clean glass substrate with photoresist. Details of the spin-coating procedure can be found in the Methods. LiPON thin film was then deposited onto the coated glass substrate by RF sputtering under N_2 plasma. After RF sputtering, LiPON sample was transferred into a container filled with Dimethyl carbonate (DMC) solvent in an argon-filled glove box. The substrate and LiPON film were fully immersed in DMC for overnight. Photoresist was then dissolved by DMC, after which LiPON film delaminated from the glass substrate and ready for pick-up. Unlike the usual way of producing LiPON thin film on a solid substrate, this method yields LiPON film in a free-standing form and exhibits transparency and remarkable flexibility as shown in **Fig. 1b** and **Supplementary Video S1**. Depending on the substrate size, deposition area and deposition time, the area, thickness and sample amount of FS-LiPON can be controlled with this procedure (**Extended Data Fig. 1**).

We performed a variety of characterizations to ensure that the structure, chemical bonding environments and electrical properties of FS-LiPON are not affected during the above synthesis procedure. The cross-sectional scanning electron microscopy (SEM) and energy-dispersive X-ray spectroscopy (EDS) elemental mapping, shown in **Extended Data Fig. 2,** demonstrate that FS-LiPON retains its fully dense nature in this 3.7-μm-thick film and that P, O, and N elements are uniformly distributed across the sample. The X-ray diffraction (XRD) results in **Extended Data Fig. 3a** indicate the amorphous characteristic of FS-LiPON. **Fig. 1c** shows the XPS result of FS-LiPON thin film; the O 1s, N 1s, P 2p and Li 1s regions manifest consistent features with substrate-based LiPON (Sub-LiPON) as shown in **Extended Data Fig. 4 & 5** and reported in the literature.[20,21] EDS elemental mapping in **Extended Data Fig. 3B** also confirm that N, P and O elements are uniformly distributed on the surface of the FS-LiPON film. In its role as a solid-state electrolyte (SSE), LiPON acts as an ionic conductor while also being an excellent electrical insulator. Electrochemical impedance spectroscopy (EIS) and direct-current (DC) polarization were subsequently employed to examine the electrical properties of FS-LiPON. The EIS spectrum in **Fig. 1d** yields an ionic conductivity of 2.5×10^{-6} S/cm for FS-LiPON, consistent with that of Sub-LiPON shown in **Extended Data Fig. 6**. DC polarization plot in **Fig. 1e** gives an electronic conductivity of 1.2×10^{-14} S/cm, on the order of that of Sub-LiPON as reported in literature.[21,22] Therefore, despite its free-standing form, FS-LiPON exhibits consistent properties with those of Sub-LiPON.

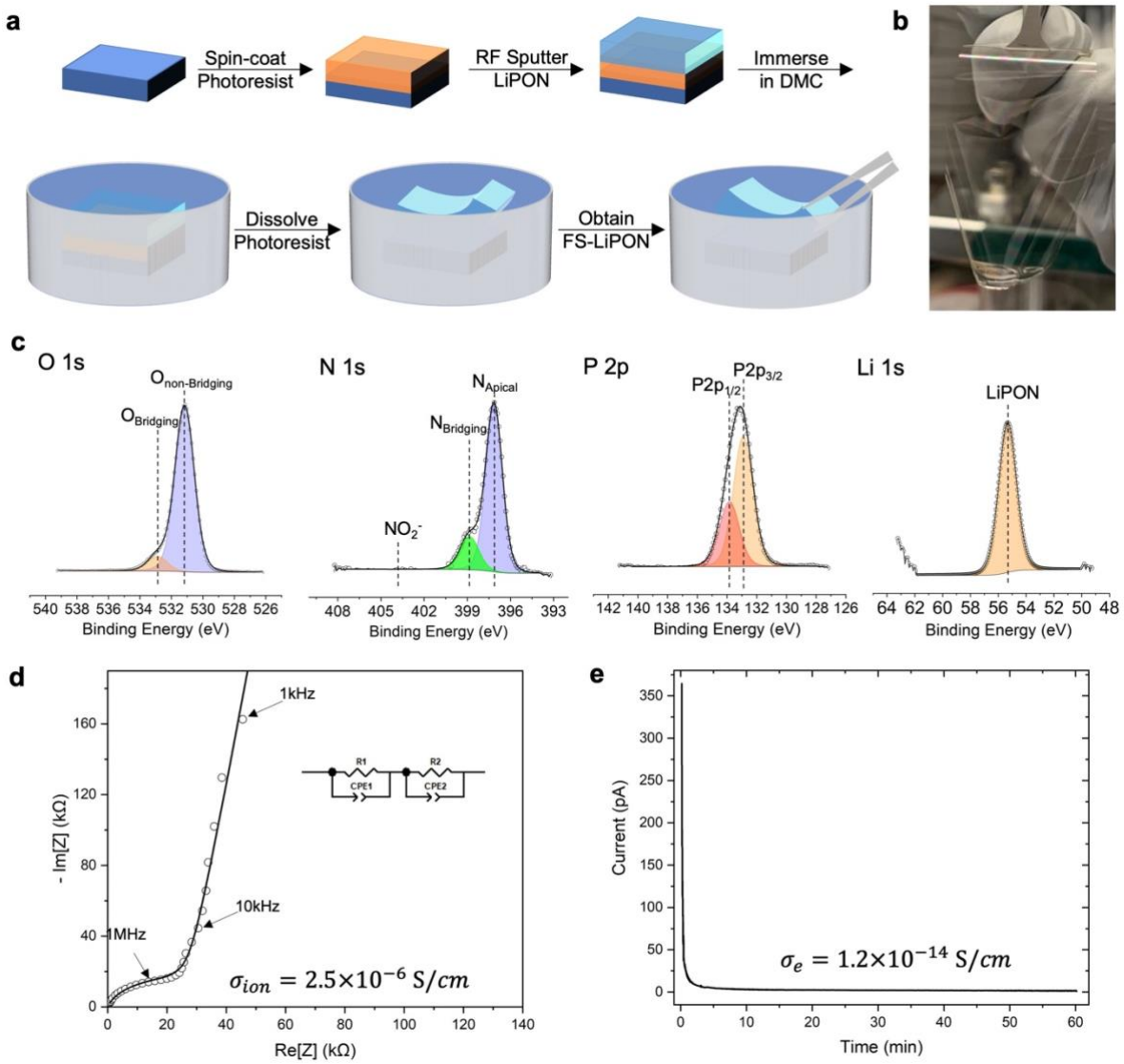

Fig 1. Synthesis procedure and basic properties examination of FS-LiPON. a, Schematic of synthesis procedure for FS-LiPON. **b,** Optical photo of a transparent and flexible FS-LiPON thin film. **c,** XPS spectra of O 1s, N 1s, P 2p and Li 1s regions of FS-LiPON thin film. **d,** EIS plot of FS-LiPON. The equivalent circuit is shown as an inset, where R1 is the ionic resistance of FS-LiPON film and CPE1 is the dielectric polarization capacitance of FS-LiPON film. R2 and CPE2 are the resistance and capacitance generated by potential interfaces between copper and FS-LiPON at medium frequency. **e,** DC polarization result of FS-LiPON.

Further Exploration of the Fundamentals of LiPON

The Li/LiPON interface remains one of the most important interfaces in the solid-state battery field and shows extraordinary electrochemical stability.[7,23] As a model example to demonstrate the advantage of using FS-LiPON for spectroscopic characterization, ss-NMR was performed on Li/FS-LiPON sample and the results are shown in **Fig. 2a-c**. The Li/FS-LiPON sample was prepared by depositing Li metal on FS-LiPON film using thermal evaporation. **Fig. 2a** shows the ^{31}P magic angle spinning (MAS) NMR spectra of FS-LiPON and Li/FS-LiPON.

A high S/N ratio of the NMR spectra was obtained, attributed to the increased sampling volume permitted by freestanding form of the samples. Based on the previous assignments for FS-LiPON,[24] four different structural units are identified in each spectrum, including orthophosphate tetrahedra PO_4^{3-} (Q^0_0), $P_2O_7^{4-}$ dimers (Q^1_0), bridging-N $P_2O_6N^{5-}$ dimers (Q^1_1) and apical-N PO_3N^{4-} units (Q^0_1). A clear difference regarding the content of these structural units is shown in **Fig. 2b**. The Li/FS-LiPON sample shows an increase (13%) of Q^0_0 units relative to the FS-LiPON sample at the expense of PON units (Q^0_1 and Q^1_1). This increase of PO_4^{3-} content indicates that a large amount of Li_3PO_4 components were generated between Li metal and LiPON as a result of interface formation, consistent with our previous observation via cryogenic electron microscopy (Cryo-EM).[7] The decrease in the other structural units such as bridging-O configuration (Q^1_0), bridging-N configuration (Q^1_1) and apical-N configuration (Q^0_1) in turn facilitate the formation of interface components such as Li_3N and Li_2O. ^{7}Li MAS NMR spectrum of Li/FS-LiPON in **Fig. 2c** shows a clear shoulder around 7.5 ppm compared with FS-LiPON, indicating Li_3N formation at the interface.[25] The slight peak shift shown in **Fig. 2c** may be due to dynamical heterogeneities between the interfacial Li ions and Li ions deep in LiPON. A Li metal signal was also clearly observed at 264 ppm in **Extended Data Fig. 7**. Previous observations by electron microscopy probed the spatial distribution of interface components between Li metal and LiPON,[7,8] while above ss-NMR results of Li/FS-LiPON sample provide quantitative insights on the content of interface components, revealing the amount of Li_3N and Li_3PO_4 formation as the interface products. The coupling of ss-NMR results with cryo-EM observation give a more complete view of the Li/LiPON interface both compositionally and spatially.

The nature of FS-LiPON also enables analysis of its thermal properties. LiPON is known to be a glassy material and the glass transition temperature is one of the most important metrics to determine the metastable states and application environments. Nevertheless, limited by the insufficient amount of active material for measurement, previously documented trials using DSC to examine the glass transition temperature of Sub-LiPON failed to capture clear transition behaviors.[26] In an attempt to compensate for this, DSC was conducted on FS-LiPON. The results in **Fig. 2d** show an obvious glass transition with an onset temperature of 207 ℃ and inflection around 234 ℃, consistent with LiPON glass transition temperature studied using spectroscopic ellipsometry.[27] Subsequent thermal response further captured the crystallization process of LiPON, along with the gas evolution observed during heating (inset images in **Fig. 2d**). DSC results suggest that LiPON should be handled at temperatures <325 ℃. Extra consideration needs to be taken when heat treatment is performed on LiPON-related

samples/devices.

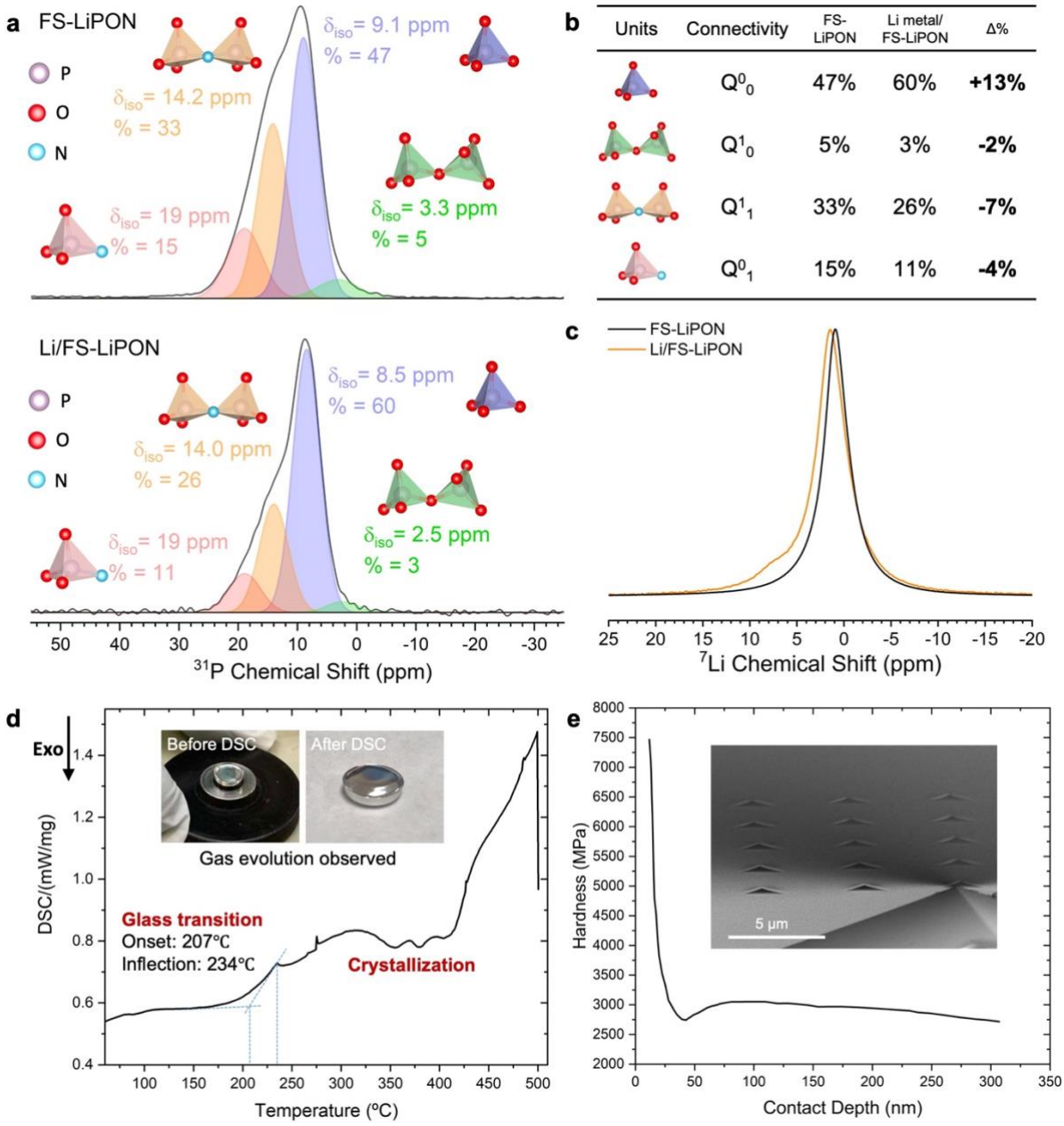

Fig. 2 Interfacial chemistry, thermal property, and mechanical properties of FS-LiPON. a, ^{31}P MAS NMR spectra of FS-LiPON and Li/FS-LiPON films. The spectrum of FS-LiPON was a reprint of our previous work[25], used here for comparison. **b,** Structural unit component differences based on NMR deconvolution. Q^0_0 stands for the orthophosphate tetrahedra PO_4^{3-} units, Q^1_0 stands for the bridging-O $P_2O_7^{4-}$ dimer units, Q^1_1 stands for the bridging-N $P_2O_6N^{5-}$ dimer units and Q^0_1 stands for the apical-N PO_3N^{4-} units. **c,** ^{7}Li MAS NMR spectra of FS-LiPON and Li/FS-LiPON d, DSC analysis of FS-LiPON film. The inset photos show the gas evolution due to DSC measurement. **e,** Film hardness values measured via continuous stiffness measurement (CSM) indentation up to ~10% of the film thickness. Inset image shows the indents array on FS-LiPON during the nanoindentation experiment using a Berkovich indenter.

Another intriguing finding lies in LiPON's mechanical properties. Note that it is essential

to maintain an inert environment during the mechanical examination of LiPON, as **Extended Data Fig. 8** and **Supplementary Video S2** show that FS-LiPON stiffened due to air exposure after 3 days. **Fig. 2e** display the nanoindentation results collected within a vacuum chamber. The hardness values were plotted against contact depth of the indenter into FS-LiPON from continuous stiffness measurement (CSM), with statistics collected from over 100 indentation locations (inset image in **Fig. 2e** shows the indents array at one sampling region). Nanoindentation gives an average hardness value around 2.7 GPa of FS-LiPON in the displacement range from 60 nm to 200 nm. The hardness values below 60 nm were primarily surface effect and have been excluded when determining the film hardness. Such a hardness of FS-LiPON is lower than the previously reported value of 3.9 GPa on sub-LiPON.[28] Based on the mathematical methods developed by Ma et al.[29] to determine Young's modulus from hardness, we obtained an average Young's modulus of FS-LiPON around 33 GPa, in contrast to the previously reported value of ~80 GPa for sub-LiPON.[28] It has been documented that vacuum deposition process commonly generates residual stress within thin film because the substrate may experience thermal expansion, contraction, or lattice mismatch, etc. during the deposition.[30] Specifically, the sputtering process tends to generate compressive residual stress in the deposited thin films, which can affect the mechanical properties, resulting in, for example, increased hardness and Young's modulus.[31] Therefore, the removal of substrate for FS-LiPON potentially releases stress within LiPON film, leading to the observed diminished hardness and Young's modulus. This observation also suggests the importance of quantifying residual stress in LiPON film before determining its mechanical properties. A series of bending tests that explore LiPON's flexibility with regard to film thickness were summarized in **Supplementary Video S3** and **Extended Data Fig. 9**.

The above results again illustrate the potential for using this free-standing film to obtain native properties of LiPON material itself. Regarding the mechanical properties, further tests such as tensile test, compression test, etc. can be performed on FS-LiPON, which would otherwise be impossible to conduct on Sub-LiPON.

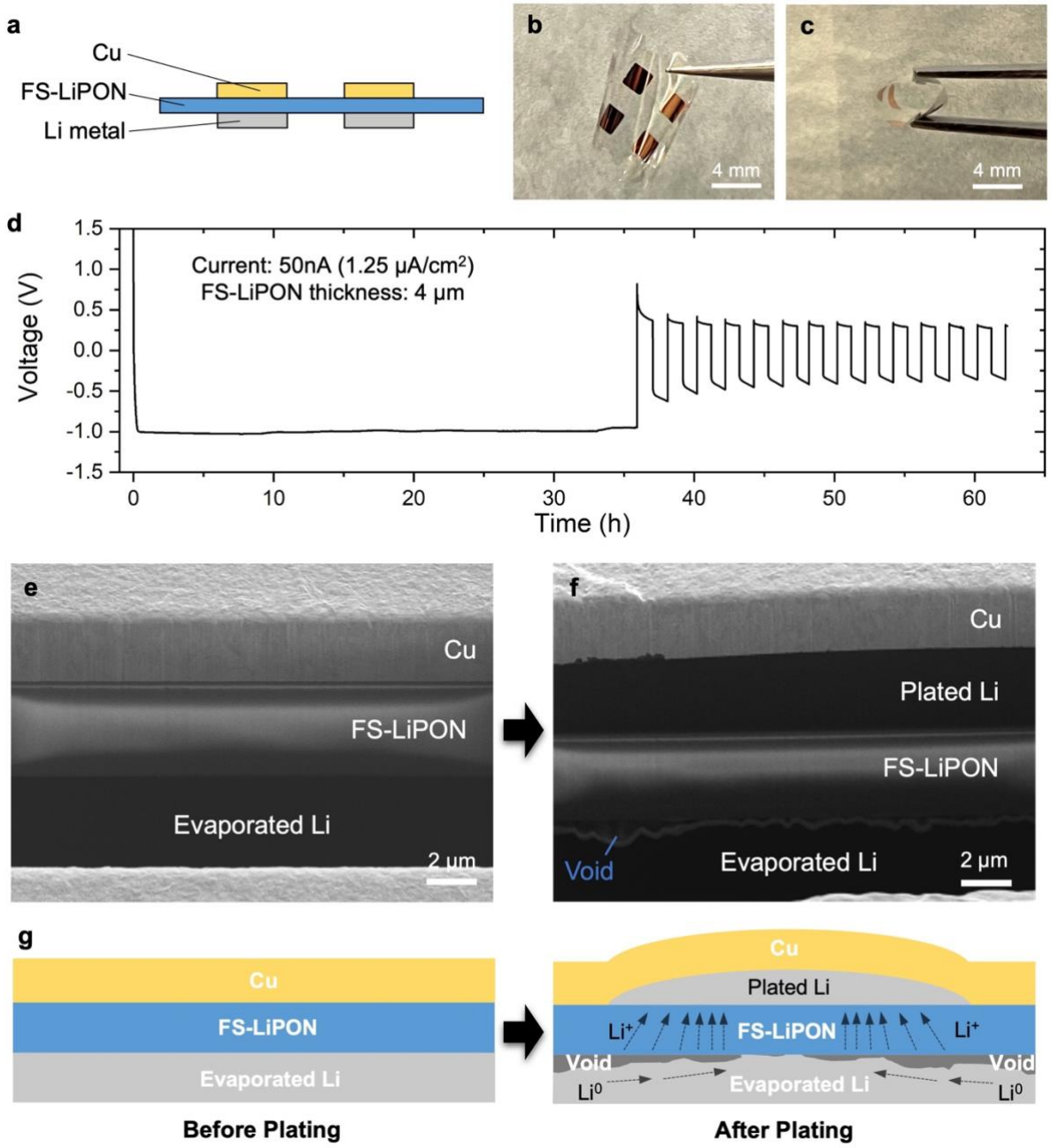

Fig. 3 Electrochemical deposition and analysis on FS-LiPON. a, Cross-section schematic of the FS-LiPON Li-Cu cell. **b,c,** Photos of FS-LiPON Li-Cu cell from top view **(b)** and upon bending **(c). d,** Voltage curve of Li metal plating and stripping in a FS-LiPON Li-Cu cell. **e, f,** Cross-section cryo-FIB/SEM images of Li-Cu cell before Li metal plating **(e)** and after Li metal plating **(f).** The plated capacity in **(f)** is ~0.31 mAh/cm^2**. g,** Schematic showing the proposed non-uniform void formation mechanism during Li metal plating.

Electrochemical Activity of FS-LiPON

Apart from its intrinsic properties, FS-LiPON is also demonstrated to be applicable in electrochemical devices. An FS-LiPON Li-Cu cell was fabricated using the configuration shown in **Fig. 3a**, where Cu and Li electrodes with the same designed area were aligned across

FS-LiPON film. As-fabricated Li-Cu cell harnesses the flexible nature of FS-LiPON as shown in **Fig. 3b**. The flexibility of the cell was further demonstrated in **Fig. 3c**, which shows how the cell can be bent by the tweezer while still able to sustain Li metal plating and stripping capability afterwards. After cell fabrication, the cell was tested using the configuration in **Supplementary Fig. 1. Fig. 3d** shows the voltage curve of the Li-Cu cell during constant-current measurement. When a current of -50 nA is applied, the cell exhibits a voltage dip and reaches an overpotential of ~-1V, after which a stable plating process proceeds. When altering the current direction, a stripping curve feature is obtained. The cell demonstrated a stable plating and stripping over 13 cycles without short-circuiting, indicating the ability of FS-LiPON to shuttle lithium ions. The relatively high overpotential is likely caused by the resistance to deformation of the Cu current collector while Li metal nucleates and grows. Apart from the nucleation barrier of Li metal, extra mechanical work is needed to overcome the Cu deformation. It is noteworthy that owing to the unique configuration of FS-LiPON Li-Cu cell, no external pressure was applied to the cycled cell.

The plated Li metal morphology in the FS-LiPON system was then examined by cryogenic focused ion beam/scanning electron microscopy (cryo-FIB/SEM). **Fig. 3e** displays the cross-section morphology of pristine Li-Cu cell, where no extra layer is observed between Cu and FS-LiPON before plating and the evaporated Li metal on the other side of FS-LiPON appears fully dense. Note that cryogenic protection during FIB milling is crucial to preserve the pristine morphology and chemistry of Li metal, as reported elsewhere before[32] and demonstrated in **Supplementary Fig. 2**. After a constant current plating, The Li-Cu cell shows a dense Li layer with dark contrast between Cu and FS-LiPON in **Fig. 3f**. The associated Li-Cu cell voltage curve is plotted in **Supplementary Fig. 3**. The EDS mapping of a plated Li-Cu cell in **Supplementary Fig. 4** illustrates the presence of Cu, P, O and Ga over corresponding regions. Such features indicate a fully dense Li metal electrochemical deposition was realized by this FS-LiPON configuration when no external pressure was present.

Intriguingly, in **Supplementary Fig. 4** a void region was observed between FS-LiPON and evaporated Li metal, as hinted by the aggregation of Ga signal that is commonly caused by redeposition during FIB milling and that is prevalently found at the bottom of void region after FIB milling.[7] A similar void feature is also observed in **Fig. 3f**, where a gap is present between FS-LiPON and evaporated Li. Although the theoretical thickness of plated Li metal is calculated to be 1.5 μm based on the areal capacity, the observing region shows a plated Li metal thickness around 4 μm in **Fig. 3f**. The top-view SEM image in **Supplementary Fig. 5** displays various bumps distributed over the Cu surface after plating. **Fig. 3g** delineates the

plating process occurring in Li-Cu cell without pressure control. Before plating, each constituent in the cell is distinguishable by the well-defined interfaces. After plating, plated Li metal forces up the Cu layer around the initial nucleation site, while the non-uniform lithium-ion flux within FS-LiPON drives lithium atoms around the vicinity of the nucleation site to migrate and compensate the metallic lithium reservoir right under the nucleation site. Therefore, void regions are formed around the nucleation site after plating is completed.

Fully Dense, Uniform Li Deposition Without External Pressure

The electrochemically deposited Li metal in other SSE systems (that is, $Li_7La_3Zr_2O_{12}$ and Li_6PS_5Cl, etc.) usually appears fully dense regardless of dendrite formation issues. This kind of morphology is likely due to the presence of external pressure on the order of several MPa.[33,34] Analogous to the cases of other solid electrolyte systems, fully dense Li metal plating has also been demonstrated in FS-LiPON system. Nevertheless, it is noteworthy that no external pressure is applied to the LiPON system, suggesting the possible presence of interfacial stress that could act as internal pressure to promote Li metal yielding and facilitate subsequent dense Li metal deposition. Previous work by Motoyama et al. proposed a model to simulate the interfacial stress between Li metal and Cu current collector after plating, where they used an imaginary Li metal sphere and estimated the radial stress on Li metal surface based on Hoop stress formula.[35]

Employing the similar stress analysis model shown in **Fig. 4a**, we applied formula (1) as follows:

$$P_i = \frac{\varepsilon_{Cu} E_{Cu}}{(1-\nu_{Cu})} \cdot \left\{ \frac{3(r_i+t)^3}{2\left[(r_i+t)^3 - r_i^3\right]} - \frac{\nu_{Cu}}{1-\nu_{Cu}} \right\}^{-1} \quad (1)$$

where P_i is the interfacial stress between Li and Cu, ε_{Cu} is strain in the circumferential directions, E_{Cu} is Young's modulus of Cu, t is the thickness of Cu, r_i is the radius of Li metal imaginary sphere, κ is the curvature of Cu, ν_{Cu} is the Poisson's ratio of Cu. The input values of above parameters were extracted from **Supplementary Fig. 6** and listed in **Supplementary Fig. 7**. **Fig. 4b** shows the Cu strain and resulting interfacial stresses in the Li-Cu cells with different Cu thickness, ranging from 0.151 GPa to 0.503 GPa as Cu strain ramps from 0.024 to 0.052. The stresses obtained here are hundreds of times higher than the external pressure applied on bulk SSE analogues. Such high interfacial stress present at Cu/Li interface confines Li metal morphology to achieve fully dense feature. Based on the stress formula given above, the interfacial stress is inversely proportional to the Li deposit diameter and proportional

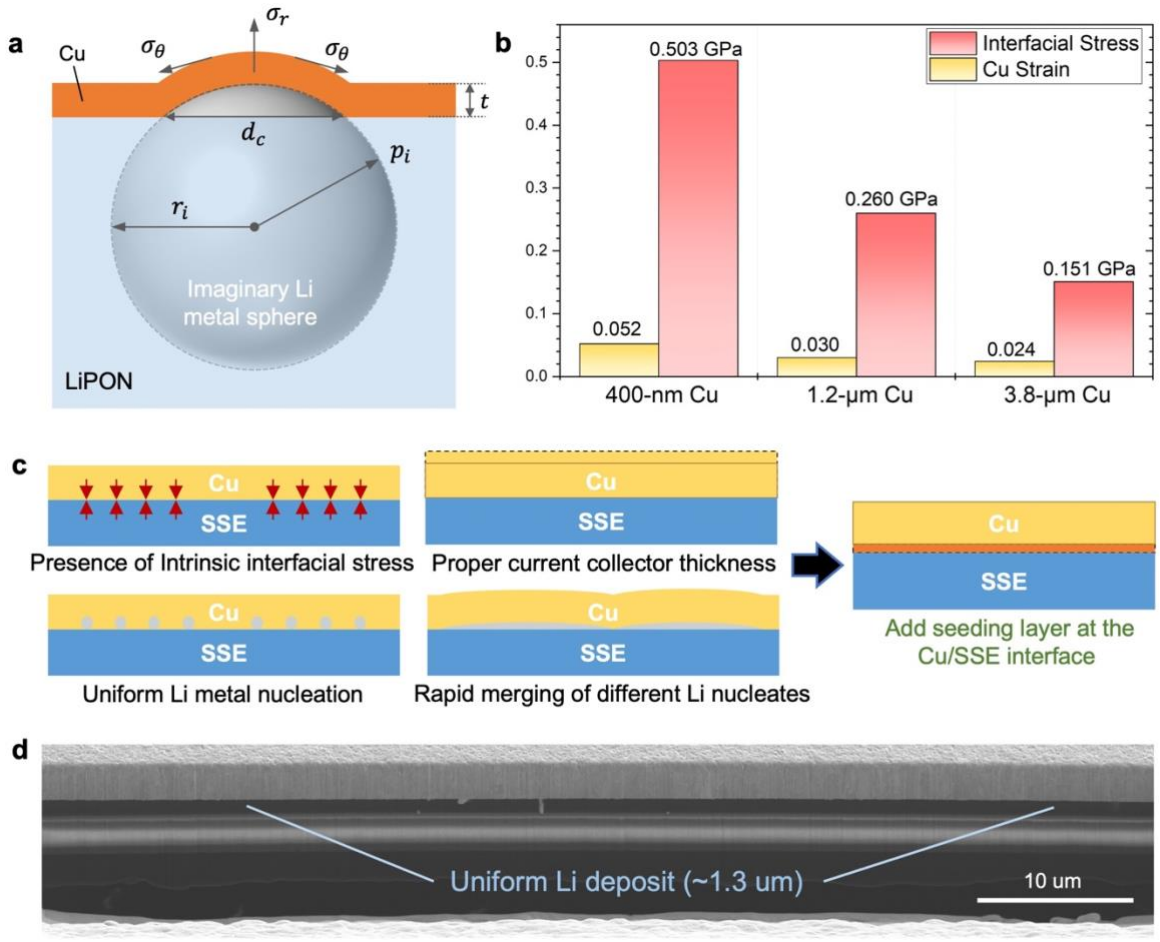

Fig. 4 Stress analysis and proposed criteria for uniform Li deposition. a, Schematic of the interface model for interfacial stress simulation, where P_i is the interfacial stress between Li and Cu, σ_θ is the stress on Cu in the circumferential directions, σ_r is the stress on Cu in the radial direction, t is the thickness of Cu, d_C is the length of the chord marked in the Li sphere underneath the Cu dome region, r_i is the radius of Li metal imaginary sphere. **b,** Cu strain and simulated interfacial stress in Li-Cu cell with regard to different Cu thicknesses. **c,** Proposed principles and solution to achieve uniform Li metal deposition in solid system. **d,** Cryo-FIB/SEM image showing uniform Li deposition realized by adding Au seeding layer in FS-LiPON Li-Cu cell.

to Cu strain, suggesting that Li metal deposit tends to have plenary growth so that overall stress can be released, resulting in more uniform coverage of Li metal on LiPON and less chance of dendrite formation. Therefore, we propose several criteria that need to be considered while building the ideal configuration for Li metal plating in solid state systems. As shown in **Fig. 4c**, intrinsic interfacial stress is essential to generate pressure during Li metal plating without the aid of external pressure; proper current collector thickness is needed to confine Li metal morphology while maintaining its own structural integrity; uniform Li metal nucleation and rapid merging of different Li nuclei help reduce the plastic deformation of current collector to prolong cyclability. Consequently, one solution to achieve uniform Li metal deposition is

adding seeding layer at Cu/SSE interface to facilitate uniform Li metal nucleation and subsequent uniform and dense Li metal growth.[36] Prior to depositing Cu on FS-LiPON, a 3-nm-thick Au layer was first evaporated on FS-LiPON. The surface SEM image and EDS results in **Supplementary Fig. 8** validates the Au film formed on FS-LiPON before Li-Cu cell fabrication. After electrochemical plating without external pressure (**Supplementary Fig. 9a**), Cu surface remains relatively smooth as shown in **Supplementary Fig. 9b**, suggesting a uniform Li metal deposition beneath. **Fig. 4d** shows a cross-section image of the Li-Cu cell with Au seeding layer after plating. The measured thickness of Li metal deposit is ~1.3 μm, close to the thickness calculated from areal capacity (**Supplementary Fig. 9a**). Li metal deposit appears not only full dense, but also uniform across the whole region. Small inclusions found in plated Li metal layer are likely the Li-Au alloy according to the cross-section EDS in **Supplementary Fig. 10**. Based on above results, with the aid of interfacial stress and seeding layer, uniform and fully dense Li metal deposition can be realized in solid-state system under zero external pressure.

Additionally, a further effort to demonstrate Li stripping in the Li-Cu FS-LiPON cell is summarized in **Supplementary Fig. 11 & 12.** Although the Li-Cu FS-LiPON cell without external pressure ended up with non-uniform stripping that led to the formation of gaps between Cu and FS-LiPON and generates inactive lithium (**Supplementary Fig. 11**), an external pressure of ~87.5 kPa helped largely improve the Coulombic efficiency to 82.7% (**Supplementary Fig. 12**). It is important to stress that external pressure appears to be essential for the stripping process, while uniformly dense Li metal plating could be realized via just interfacial stress and a seeding layer. An intriguing observation was that the gap/void caused by stripping was formed between Cu and Li metal instead of being present between Li metal and FS-LiPON (**Supplementary Fig. 12**), in contrast to the scenarios reported in bulk solid-state systems using argyrodite- or garnet-type SSEs.[37,38] This difference is indeed related to the various current densities applied. Nevertheless, the fact that void was absent between Li metal and SSE in this case might be related to LiPON's unique amorphous characteristic and its electrochemical stability against Li metal.

Conclusions

This work presents a methodology to produce a thin film LiPON in a free-standing form that is transparent and demonstrates remarkable flexibility. The absence of substrate enables fundamental studies of LiPON and the Li/LiPON interface by ss-NMR. DSC captures the glass

transition behavior of LiPON around 207 °C with a high signal-to-noise ratio. Nanoindentation and flexibility test yield a Young's modulus of ~33 GPa of LiPON and show the flexible nature of LiPON film, respectively. An electrochemical cell employing FS-LiPON shows its ability to conduct lithium ions. Stress analysis at Li/Cu interface suggests the presence of a high compressive stress in the order of 10^{-1} GPa, which facilitates Li metal yielding and a dendrite-free, dense Li metal morphology. Using a gold seeding layer, we realize a fully dense and uniform Li metal deposition under zero external pressure. These conditions, combining interfacial stress and a seeding layer, are ideal for uniform Li metal deposition . The amorphous nature and interfacial stability of LiPON prevents void formation within Li metal deposits during the stripping process. We believe that this free-standing form of LiPON thin films will lead to a wider application of LiPON material. When coupled with casted cathodes, FS-LiPON can potentially enable Li metal anode deposition with minimal external pressure.

Acknowledgements

We gratefully acknowledge funding support from the U.S. Department of Energy, Office of Basic Energy Sciences, under Award Number DE-SC0002357. FIB/SEM in this work was performed in part at the San Diego Nanotechnology Infrastructure (SDNI) of UCSD, a member of the National Nanotechnology Coordinated Infrastructure, which is supported by the National Science Foundation (Grant ECCS-2025752). NMR was performed under the auspices of the US Department of Energy by LLNL under contract number DE-AC52-07NA27344. XPS and DSC were performed at the UC Irvine Materials Research Institute (IMRI) using instrumentation funded in part by the National Science Foundation Major Research Instrumentation Program under grant no. CHE-1338173 and DMR-2011967.

Author Contributions

D.C., M.Z. and Y.S.M conceived the ideas. D.C., T.W., B.L., R.S. and B.S. prepared the thin film sample. The FS-LiPON Li-Cu cell was designed by D.C. B.H., M.Z. and G.Z., and fabricated by D.C. M.M. performed and analyzed ss-NMR measurements. D.C. conducted cryo-FIB/SEM and electrical measurements. D.C. and H.N. collected XRD data. D.C., J.B. and P.H. collected and analyzed the nanoindentation data. D.C., Y.Y. and W.L. collected XPS data. D.C., M.Z., Y.S.M., T.W., M.M., G.Z. and B.H. co-wrote the paper. All authors discussed the results and commented on the paper. All authors have approved the final paper.

Declaration of Interests

The authors declare no competing interests.

References

1. Yu, X., Bates, J. B., Jellison, G. E. & Hart, F. X. A Stable Thin-Film Lithium Electrolyte: Lithium Phosphorus Oxynitride. *J. Electrochem. Soc.* **144**, 524 (1997).
2. J.B. Bates, N.J. Dudney, G.R. Gruzalski, R.A. Zuhr, A. Choudhury, C. F. L. Electrical properties of amorphous lithium electrolyte thin films. *Solid State Ionics* **29**, 42–44 (1992).
3. Lacivita, V. *et al.* Resolving the Amorphous Structure of Lithium Phosphorus Oxynitride (Lipon). *J. Am. Chem. Soc.* **140**, 11029–11038 (2018).
4. Santhanagopalan, D. *et al.* Interface limited lithium transport in solid-state batteries. *J. Phys. Chem. Lett.* **5**, 298–303 (2014).
5. Wang, Z. *et al.* In situ STEM-EELS observation of nanoscale interfacial phenomena in all-solid-state batteries. *Nano Lett.* **16**, 3760–3767 (2016).
6. Wang, Z. *et al.* Effects of cathode electrolyte interfacial (CEI) layer on long term cycling of all-solid-state thin-film batteries. *J. Power Sources* **324**, 342–348 (2016).
7. Cheng, D. *et al.* Unveiling the Stable Nature of the Solid Electrolyte Interphase between Lithium Metal and Lipon Via Cryogenic Electron Microscopy. *Joule* **4**, 2484–2500 (2020).
8. Hood, Z. D. *et al.* Elucidating Interfacial Stability between Lithium Metal Anode and Li Phosphorus Oxynitride via in Situ Electron Microscopy. *Nano Lett.* **21**, 151–157 (2021).
9. Lewis, J. A., Tippens, J., Cortes, F. J. Q. & McDowell, M. T. Chemo-Mechanical Challenges in Solid-State Batteries. *Trends Chem.* 1–14 (2019) doi:10.1016/j.trechm.2019.06.013.
10. Herbert, E. G., Tenhaeff, W. E., Dudney, N. J. & Pharr, G. M. Mechanical characterization of LiPON films using nanoindentation. *Thin Solid Films* **520**, 413–418 (2011).
11. Xu, F. *et al.* Complete elastic characterization of lithium phosphorous oxynitride films using picosecond ultrasonics. *Thin Solid Films* **548**, 366–370 (2013).
12. Zhao, S., Fu, Z. & Qin, Q. A solid-state electrolyte lithium phosphorus oxynitride film prepared by pulsed laser deposition. *Thin Solid Films* **415**, 108–113 (2002).
13. Kozen, A. C., Pearse, A. J., Lin, C. F., Noked, M. & Rubloff, G. W. Atomic Layer Deposition of the Solid Electrolyte LiPON. *Chem. Mater.* **27**, 5324–5331 (2015).
14. Liu, W. Y., Fu, Z. W., Li, C. L. & Qin, Q. Z. Lithium phosphorus oxynitride thin film fabricated by a nitrogen plasma-assisted deposition of E-beam reaction evaporation. *Electrochem. Solid-State Lett.* **7**, 36–41 (2004).
15. Nowak, S., Berkemeier, F. & Schmitz, G. Ultra-thin LiPON films - Fundamental properties and application in solid state thin film model batteries. *J. Power Sources* **275**, 144–150 (2015).
16. Kim, H. T., Mun, T., Park, C., Jin, S. W. & Park, H. Y. Characteristics of lithium phosphorous oxynitride thin films deposited by metal-organic chemical vapor deposition technique. *J. Power Sources* **244**, 641–645 (2013).
17. Muñoz, F. *et al.* Increased electrical conductivity of LiPON glasses produced by ammonolysis. *Solid State Ionics* **179**, 574–579 (2008).
18. Westover, A. S. *et al.* Plasma Synthesis of Spherical Crystalline and Amorphous

Electrolyte Nanopowders for Solid-State Batteries. *ACS Appl. Mater. Interfaces* **12**, 11570–11578 (2020).

19. López-Aranguren, P. *et al.* Crystalline LiPON as a Bulk-Type Solid Electrolyte. *ACS Energy Lett.* 445–450 (2021) doi:10.1021/acsenergylett.0c02336.
20. Schwöbel, A., Hausbrand, R. & Jaegermann, W. Interface reactions between LiPON and lithium studied by in-situ X-ray photoemission. *Solid State Ionics* **273**, 51–54 (2015).
21. Bates, J. B. *et al.* Fabrication and characterization of amorphous lithium electrolyte thin films and rechargeable thin-film batteries. *J. Power Sources* **43**, 103–110 (1993).
22. Le Van-Jodin, L., Ducroquet, F., Sabary, F. & Chevalier, I. Dielectric properties, conductivity and Li+ ion motion in LiPON thin films. *Solid State Ionics* **253**, 151–156 (2013).
23. Li, J., Ma, C., Chi, M., Liang, C. & Dudney, N. J. Solid electrolyte: The key for high-voltage lithium batteries. *Adv. Energy Mater.* **5**, 1–6 (2015).
24. Marple, M. A. T. *et al.* Local Structure of Glassy Lithium Phosphorus Oxynitride Thin Films: A Combined Experimental and Ab Initio Approach. *Angew. Chemie - Int. Ed.* **59**, 22185–22193 (2020).
25. Köcher, S. S. *et al.* Chemical shift reference scale for Li solid state NMR derived by first-principles DFT calculations. *J. Magn. Reson.* **297**, 33–41 (2018).
26. M. F. Vieira, E. *et al.* Flexible solid-state Ge – LiCoO2 battery: From materials to device application. *Adv. Mater. Lett.* **8**, 820–829 (2017).
27. Sepúlveda, A., Criscuolo, F., Put, B. & Vereecken, P. M. Effect of high temperature LiPON electrolyte in all solid state batteries. *Solid State Ionics* **337**, 24–32 (2019).
28. Kalnaus, S., Westover, A. S., Kornbluth, M., Herbert, E. & Dudney, N. J. Resistance to fracture in the glassy solid electrolyte Lipon. *J. Mater. Res.* 1–10 (2021) doi:10.1557/s43578-020-00098-x.
29. Ma, D., Chung, W. O., Liu, J. & He, J. Determination of Young's modulus by nanoindentation. *Sci. China, Ser. E Technol. Sci.* **47**, 398–408 (2004).
30. Abadias, G. & Daniel, R. *Stress in physical vapor deposited thin films: Measurement methods and selected examples*. *Handbook of Modern Coating Technologies* (BV, 2021). doi:10.1016/b978-0-444-63239-5.00008-1.
31. Swadener, J. G., Taljat, B. & Pharr, G. M. Measurement of residual stress by load and depth sensing indentation with spherical indenters. *J. Mater. Res.* **16**, 2091–2102 (2001).
32. Lee, J. Z. *et al.* Cryogenic Focused Ion Beam Characterization of Lithium Metal Anodes. *ACS Energy Lett.* **4**, 489−493 (2019).
33. Wang, M. J., Carmona, E., Gupta, A., Albertus, P. & Sakamoto, J. Enabling "lithium-free" manufacturing of pure lithium metal solid-state batteries through in situ plating. *Nat. Commun.* **11**, 1–9 (2020).
34. Lee, Y. G. *et al.* High-energy long-cycling all-solid-state lithium metal batteries enabled by silver–carbon composite anodes. *Nat. Energy* **5**, 299–308 (2020).
35. Motoyama, M., Ejiri, M. & Iriyama, Y. Modeling the Nucleation and Growth of Li at Metal Current Collector/LiPON Interfaces. *J. Electrochem. Soc.* **162**, A7067–A7071 (2015).
36. Yan, K. *et al.* Selective deposition and stable encapsulation of lithium through heterogeneous seeded growth. *Nat. Energy* **1**, 16010 (2016).

37. Lee, K., Kazyak, E., Wang, M. J., Dasgupta, N. P. & Sakamoto, J. Analyzing void formation and rewetting of thin in situ-formed Li anodes on LLZO. *Joule* **6**, 2547–2565 (2022).
38. Kasemchainan, J. *et al.* Critical stripping current leads to dendrite formation on plating in lithium anode solid electrolyte cells. *Nat. Mater.* **18**, 1105–1111 (2019).

Methods

Photoresist Spin Coating

AZ1512 photoresist (from EMD Performance Materials Corp.) is coated on clean glass substrate by spin coating. The heater temperature for prebake and postbake was set as 100℃. The spinning recipe includes 500 RPM for 20s, 1000 RPM for 20s and 2000 RPM for 60s. The resulting photoresist layer thickness is about 1.7 μm, followed by UV light treatment for ~1 min.

Thin Film Deposition

LiPON thin film was deposited on photoresist-coated glass substrate by RF sputtering using a crystalline Li_3PO_4 target (2″ in diameter, from Plasmaterials, Inc.) in UHP nitrogen atmosphere. The base pressure of the sputtering system was 3.0×10^{-6} Torr. LiPON deposition used a power of 50W and nitrogen gas pressure of 15 mTorr. The as-deposited LiPON thin film was 3.7 μm in thickness with a growth rate of ~0.46 Å/s. The copper pads for EIS tests and current collector were deposited by thermal evaporation using copper pellets (from Kurt J. Lesker, 99.99% purity). Growth rate is 1 Å/s. Li metal anode for the Li-Cu cell was deposited by thermal evaporation with a base pressure of 2.5×10^{-8} Torr and growth rate of 3-4 Å/s. The Au seeding layer was deposited by thermal evaporation using gold pellets (from Kurt J. Lesker, 99.99% purity). Growth rate is 1.5 Å/s.

X-Ray Diffraction

The powder crystal X-ray diffraction was carried out on a Bruker micro focused rotating anode, with double bounced focusing optics resulting in Cu $K_{\alpha1}$ and $K_{\alpha2}$ radiation (λ_{avg} =1.54178 Å) focused on the sample. A sample of FS-LiPON was mounted onto a four circle Kappa geometry goniometer with APEX II CCD detector.

Microscopic Morphology and Chemical Analysis

Scanning Electron Microscopy (SEM) was performed using an FEI Apreo SEM with an electron beam energy of 5 keV and an electron beam current of 0.1 nA. The energy dispersive spectroscopy X-Ray spectroscopy (EDS) was collected using an electron beam energy of 5 keV by the Pathfinder EDS software from Thermo Scientific.

X-ray Photoelectron Spectroscopy

X-Ray photoelectron spectroscopy (XPS) was performed in an AXIS Supra XPS by Kratos Analytical. XPS spectra were collected using a monochromatized Al Kα radiation (hυ = 1486.7 eV) under a base pressure of 10^{-9} Torr. To avoid moisture and air exposure, a nitrogen filled glovebox was directly connected to XPS spectrometer. All XPS measurements were collected with a 300 × 700 μm^2 spot size. Survey scans were performed with a step size of 1.0 eV, followed by a high-resolution scan with 0.1 eV resolution, for lithium 1s, carbon 1s, oxygen 1s, nitrogen 1s, and phosphorous 2p regions. A 5 keV Ar plasma etching source was used for surface etching with a pre-etching for 5 s, etching for 60 s and post-etching for 10 s. All spectra were calibrated with adventitious carbon 1s (284.6 eV) and analyzed by CasaXPS software.

Electrochemical Measurements

A Biologic SP-200 potentiostat was used to measure the electrochemical impedance spectroscopy (EIS) and DC polarization of FS-LiPON, and electrochemical cycling of Li-Cu FS-LiPON cells. The frequency range for EIS was 3 MHz to 100 mHz with an amplitude of 10 mV and the obtained data fitted with a linear least square fitting method. The constant voltage used for DC polarization is 1V. The setup for electrochemical measurement is shown in the schematic in Supplementary Fig. 6a and 10. To apply external pressure on Li-Cu FS-LiPON cell, a rigid stainless-steel plate (2×2×0.03 mm^2) was placed between the active region of the cell and the probe during measurements.

Solid-state Nuclear Magnetic Resonance

The NMR measurements performed on FS-LiPON and Li/FS-LiPON were collected using a 2.5 mm H/X/Y channel Bruker probe on a 600 MHz Bruker Biospin Avance III, operating at 242.94 and 233.25 MHz for ^{31}P and ^{7}Li. The samples were packed within a 2.5 mm pencil-type ZrO_2 rotor and spun at 25 kHz. The ^{31}P spectra were collected as a rotor synchronized Hahn echo experiment with a 90° pulse of 2.54 μs (B_1 field strength ~98 kHz). The Hahn echo experiments were processed from the top of the echo to remove the effects of ring down from the FID. A single pulse experiment with a pulse length of 2.875 μs (B_1 field strength ~87 kHz) was used to acquire the ^{7}Li spectra. The recycle delays used for the 1D experiments was 60 s

for ^{31}P and 2 s for ^{7}Li.

Differential Scanning Calorimetry

The Differential Scanning Calorimetry (DSC) measurement was conducted with DSC 214 Polyma (Netzsch). The temperature range was from 50°C to 500°C with a heating rate of 10°C /min. The DSC measurement was conducted under N_2 environment. All samples were sealed in aluminum pans in an Argon-filled glovebox to reduce contamination.

Nanoindentation

Nanoindentation was performed inside of a Thermo Fisher Scientific Scios 2 DualBeam FIB/SEM using a FemtoTools FT-NMT04 nanoindenter equipped with a Berkovich tip. Measurements of hardness and reduced modulus employed the continuous stiffness measurement (CSM) technique using a displacement-controlled test. Mechanical property values were averaged between displacements of ~60 nm and ~200 nm. Several five-by-five indent arrays were performed at various locations on FS-LiPON films that were bonded to SEM stubs using epoxy. Tests were performed using a 4 s load-ramp time and a 0.2 s unload-ramp time. When transferring samples from an inert environment to the Scios 2 SEM, samples were exposed to <120s of atmosphere prior to the vacuum conditions inside the SEM.

Cryogenic Focused Ion Beam/Scanning Electron Microscopy

A FEI Scios DualBeam FIB/SEM equipped with cryo-stage was used to observe the surface and cross-section morphology of plated Li metal in FS-LiPON Li-Cu cell. The operating voltage of electron beam was 5 kV. Emission current of electron beam was set to 25 pA to minimize potential damage of electron beam. A gallium ion beam source was used to mill and thin the sample. The operating voltage of ion beam source was 30 kV. Emission currents of ion beam were chosen for different purposes, i.e., 10 pA for imaging by ion beam, 0.1 nA for cross-section cleaning and 3 nA for pattern milling. To preserve the Li metal pristine morphology, a cryo-stage was used during pattern milling and cross-section cleaning processes, where the temperature of cryo-stage was maintained at around -185°C due to heat exchanging with cooled nitrogen gas.

Data availability

Additional data related to this paper are available from the corresponding authors upon reasonable request.